A MICRO TESLA TURBINE FOR POWER GENERATION FROM LOW PRESSURE HEADS AND EVAPORATION DRIVEN FLOWS

Vedavalli G. Krishnan[1], Zohora Iqbal[1] and Michel M. Maharbiz[1]
[1]University of California Berkeley, CA., US

ABSTRACT

We report on the design, fabrication and testing of a low pressure head Tesla microturbine. We began developing this technology as a means of scavenging energy from fluids flows induced in plant-like evaporative systems. Unlike traditional inertial turbines, Tesla turbines have high efficiency when driven with low pressure flows, are relatively simple to manufacture and scale down very favorably. The 1 cm^3 rotor diameter turbine presented here is, to our knowledge, the smallest Tesla turbine reported, with an unloaded peak power of 45 mW (12 cc/sec flow, 17% efficiency) and a peak efficiency of 40% (< 2 cc/sec flow). Moreover, the entire turbine is built using a variety of modern commercial rapid prototyping methods, making its construction accessible to almost anyone. Beyond applications in evaporative scavenging, Tesla microturbines may find use as components in ultrasmall-profile heat engines and for energy generation from sources of low pressure head flow.

KEYWORDS

Tesla turbine, viscous turbine, miniaturize turbine, power MEMS, microturbine.

INTRODUCTION

The cohesive properties of water enable the ascent of sap to the top of trees against gravity and frictional losses, driven by evaporation at microscale pores in leaves. For a 100 m tree, this corresponds to a minimum pressure difference of 10 bars between leaf and root [1], and with a plant evaporation rate of 5nl/cm^2/sec, a power of 15µW/cm^2 and an 'energy density' of 3 kJ per kg of evaporated water. Earlier work scavenged energy from evaporation-induced water flows by charging pumping a circuit via dielectric-water interface transition between capacitor plates [2]. In this work, we present a microturbine which can be driven by evaporative flow (Figure 1).

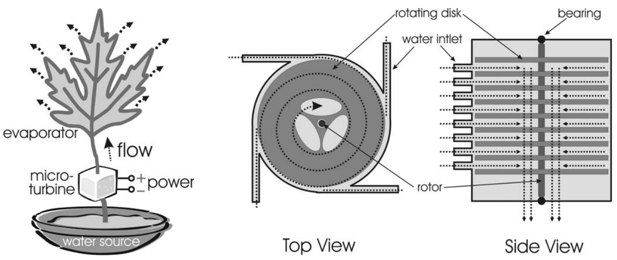

Figure 1 (left) power generation concept;(right) turbine concept. Fluid entering through the inlets spirals inwards between disks, transferring power to the rotor shaft. Fluid exists through holes near the center of each disk and downwards out of the turbine.

Our aim is to design miniaturized turbines (1 – 25 mm diameter) that are capable of producing 1 mw – 10 W power outputs. The 10 mm diameter turbines we present here operate at low Reynolds numbers (NRE ~ 1 – 15) corresponding to laminar flow and they transfer energy using the drag force of viscosity and the adhesive nature of the flowing fluid. At micro-scale, the surface area-to-volume ratio increases and surface tension, adhesion, and cohesion forces play a bigger role compared to inertial forces. Thus, rotors that use kinematic viscosity and surface effects (rather than inertia) become a good choice for micro-scale power extraction machinery. Previous research work on turbine scale-down by R.T. Deam et al. [4] has shown that viscous turbines outperform conventional impact-based turbines as they are scaled down to millimeter range. In this paper we present background, theory, fabrication and test results of our turbines.

THEORY AND SIMULATION

Basic operation of 'Tesla' turbines

In Tesla turbines (Figure 1, right), the adhesion and viscosity of a moving medium are used to propel closely spaced disks into rotation. The fluid enters the inner space between the disks from the periphery and exits through central holes near the axle (dotted lines). There are no constraints or obstacles intended to couple inertial forces (i.e. vanes) as in traditional turbines. The fluid enters tangentially at the periphery and makes several revolutions while spiraling towards the central exhaust (dotted lines). During this process, it transfers momentum to the disks. Under ideal conditions, there is no slippage between the tip velocity of the rotating disks and the tangential velocity of the fluid entering the disks at the nozzle exit. The efficiency of energy transfer is largely governed by the smoothness of the medium flow from the nozzle to the disks (effectively a fluidic impedance matching problem), the effectiveness of the bearing in reducing the friction loss, and the size of the active area for the transfer of the momentum.

Theoretical efficiency

We measure the turbines expansion efficiency, also known as isentropic or component efficiency. Here the work output is derived from the moment of inertia of the rotor and the rotor acceleration and deceleration characteristic at a given flow rate. The work input is calculated from the flow rate and the pressure drop across the turbine.

W. Rice [5] published the first extensive theoretical work on Tesla turbines, providing results from numerical simulations of fluid-disk interactions. More recently, Romanin et al. have provided analytical solutions for Tesla turbine operation suitable for the regimes tested here [6].

From Rice et al., the theoretical fluidic-to-mechanical rotor efficiency can be as high as 80%. The performance is governed by the rotor, nozzle and fluid characteristics. Rotor radius, exhaust/rotor radius ratio, and exhaust area. govern the effective rotor area. The nozzle dimensions and nozzle positioning affects the nozzle loss and the nozzle-to-rotor interactions. The kinematic viscosity and density of the fluid influences the energy transfer. The bearing and any seals influence the losses. The flow rate controls the power output and the smoothness of the flow.

A complete description of the analysis is outside the scope of this paper; see [5, 6]. Applying the Rice et al. results to our system, theoretical specific power was calculated for a 1 cm diameter rotor with 20 disks spaced 125 µm apart (Figure 2). Table 1 compares the predicted performance of three different systems: a *micro* turbine (1 mm disk diameter), a *mini* turbine (1 cm disk diameter), and a *mini* turbine driven with 20 cm^3/sec steam at 0.1 bar pressure.

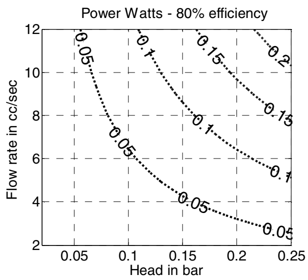

Figure 2: Theoretical maximum specific power (W/cm^3) at a range of flow and pressures for a 1 cm, 20 disk, 125µm spacing rotor

Table 1: Specifications and theoretical performance

System	Flow	Diameter	Spacing	Isentropic Efficiency	Power	Power density
	volume/s	*mm*	*µm*	*%*	*mW*	*mW/cc*
micro	5µl	1	25	78	0.04	8
mini-W	4cc	10	125	74	31	60
mini-S	20cc	10	125	45	1450	2680

FABRICATION AND TESTING

Turbine fabrication and assembly

Disks of 1 and 2 cm diameters with three different center exhaust hole patterns were fabricated using commercial photo etching (Microphoto, Inc., Roseville, MI) on 125 µm thick, 300 series full hard stainless steel sheets (Figure 3, Table 2). A square axle with rounded ends was used to enable automatic alignment of the disks. The spacers were 125 µm thick.

We assembled four different rotor stacks with 1 cm diameter disks: two with 125 µm inner disk spacing but with different exhaust holes designs, one with 250µm spacing, and one with 500µm spacing. The number of disks in the rotor assemblies varied (20, 13 and 8, respectively) to fit in the same enclosure. The rotors were held tight by two screws on either side. Ruby Vee bearings (1.25 mm OD, Bird Precision, Waltham, MA) connect the shaft to the housing. These perform well at <10000 RPM.

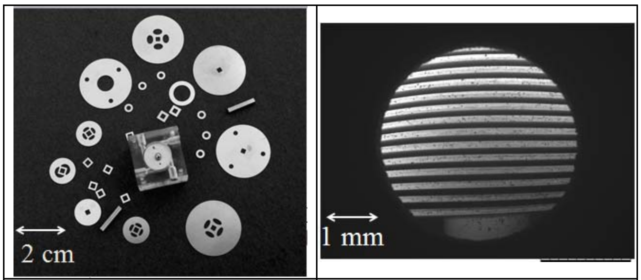

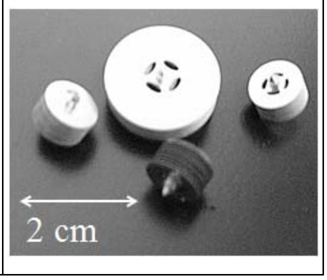

Figure 3: (top left) various photo-etched stainless steel disks, bronze square axle; (top right) white light microscopy (20x) showing 125 µm disk and post-assembly gap uniformity of rotor stack. (bottom right) assembled three 1cm and 2 cm rotors

Table 2: Rotor Specifications

Rotor	Disks	Gap	Exhaust/Rotor radius	Exhaust/Disk Area
1	*20*	*h =125 µm*	$r_i / r_o = 0.47$	*0.105*
2	*20*	*h =125 µm*	$r_i / r_o = 0.51$	*0.143*
3	*13*	*h =250 µm*	$r_i / r_o = 0.47$	*0.105*

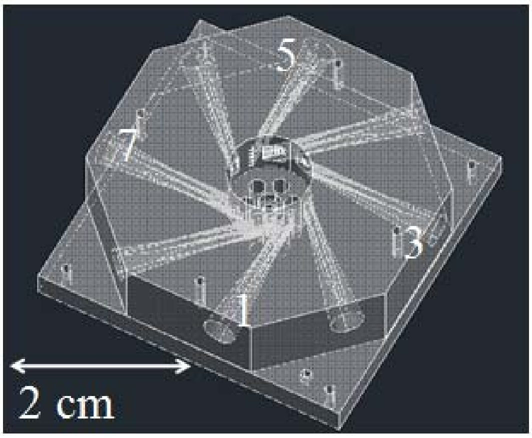

Figure 4: CAD view of enclosure with the 8 nozzles tested. Center rotor housing diameter:1.013 cm All noz entry holes diameter :4.04 mm; Nozzle exit info:

Table 3: Nozzle Specifications

Nozzle	Type	Inlet Area (% of rot area)	Area (mm_2)	Inlet angle (° to tangent)
4,8	*Converging circular*	*4%*	*3.28*	*0*
1,2,6	*Converging circular*	*4%*	*3.28*	*15,25,35*
3	*Converging circular*	*2.9%*	*2.28*	*0*
5	*Circular array*	*0.8%*	*0.69*	*15*
7	*funnel*	*9%*	*7.14*	*15*

Nozzle impedance mismatch is known to contribute to large performance degradation in turbines and is especially important for turbine of this kind [3, 5]. To explore the nozzle parameter space, we used 3D plastic rapid prototyping (ProtoTherm 12120 polymer, 0.002" layer thickness, High-Resolution Stereolithography 3, FineLine Prototyping, Inc., Raleigh, NC) which allowed us to build designs which would otherwise be un-machinable. Seven different nozzle types (Figure 4, Table 3) were tested on rotor performance.

Testing and characterization

Figure 5 shows the test setup. A gear pump (EW-74014-40, Cole-Parmer Instrument Company, Vernon Hills, IL) was used to produce 1 – 20 cm^3/sec flow rates while the pressure at the nozzle inlet was measured (DPG8000-100, Omega Engineering, Inc, Stamford, CT). During operation, the rotation of the turbine was recorded using a high speed video camera (FASTCAM-X 1024PCI, Photron, San Diego, CA using PFC Viewer software). Thermocouples at the top and bottom of the enclosure (5SC-TT-K-40-36, Omega Engineering, Inc., Stamford, CT) monitored turbine temperature.

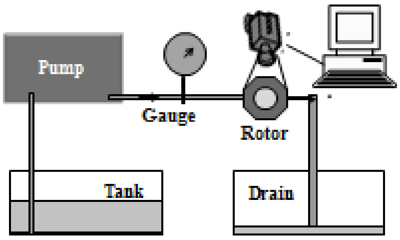

Figure 5: Gear pump draws water from a tank and drives the rotor. The nozzle inlet pressure is measured using a gauge and the rotor movement is recorded using high speed camera.

TEST RESULTS AND DISCUSSION

Test data and operation verification

Eight systems with different nozzle and 1cm rotors are tested with the pump system as shown in Figure 5

Pressure vs. flow rate measurements were carried out for all the systems (Figure 6). It is observed that the pressure head for a particular flow is mainly determined by the nozzle and the three different rotors produced only small variations in the pressure head.

The Reynolds number (N_{RE}) is calculated using the rotor spacing and RPM at flow rates from 2 cc/sec to 20 cc/sec; it is < 15 for the 20 disk stacks and < 40 for the 13 disk stacks (Figure 6).

$$N_{RE} = 2 \pi f \rho h^2 / \nu \qquad (1)$$

Where ν is the kinematic viscosity, ρ is the density, f is the rotor revolution/sec, and h is the space between the disks. For our pressures and flows, Reynolds numbers varied from 0.5 to 12 for 20 disk rotors R1 and R2; It varied 2 - 42 for 13 disk stacks with double the disk gap.

In all but one case, only *one nozzle* was used to inject fluid during operation (see also *Summary*). The tested systems specifications are listed in Table 4, along with peak performance. Maximum performance for the first four systems is in Table 5; the maximum power output with nozzle 3 and rotor 2 (N3-R2) was 55mW at 9% efficiency whereas nozzle 4 with rotor 1 (N4-R1) had the best performance of power out of 45mW at 17.3% efficiency.

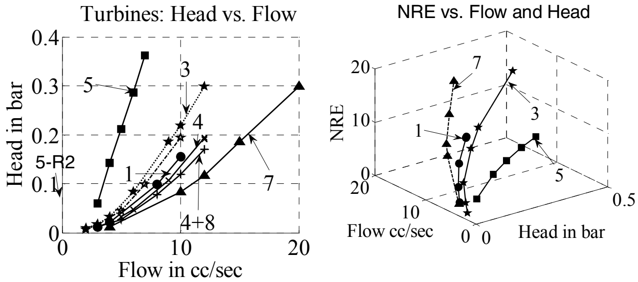

Figure 6: (left) Pressure head vs. flow for the eight systems tested. (right) Reynolds number for the tested nozzles at different flow rate and heads for rotor 1.

*Table 4: **Six** different nozzles and **three** different rotors **were** tested. **Data from N3-R3** is used **for Figures 8-10**; see Table 2 for rotor **specifications**.*

Nozzle# Rotor#	Flow (cc/s)	P (bar)	Rotation (rpm)	NRE	Power (mW)	eff (%)
N1-R1	9	0.11	3499	5.7	10.1	10.5
N3-R1	8	0.15	5590	9.3	20.3	18.4
N3-R2	8	0.13	5264	8.6	19.8	19.7
N3-R3	10	0.19	6522	43	16.9	9.3
N4-R1	**12**	**0.23**	**7247**	**12**	**45.0**	**17.3**
N4+8-R1	**14**	**0.19**	**6977**	**11**	**29.0**	**10.9**
N5-R1	6	0.29	4639	7.6	13.0	8.1
N7-R1	12	0.17	5807	9.5	23.2	11.9

Table 5: Maximum efficiency for four systems. As expected, highest efficiencies are achieved at lower flow rates and pressure (see Figure 10).

Nozzle# Rotor#	Flow (cc/s)	P (bar)	Rotation (rpm)	NRE	Power (mW)	eff (%)
N3-R3	**2**	**0.01**	**1243**	**8.1**	**0.4**	**36.6**
N3-R2	2	0.01	689	1.1	0.32	27.0
N3-R1	5	0.06	3488	5.7	0.87	22.0
N1-R1	6	0.05	2190	3.6	3.6	12.5
N3-R2	**15**	**0.43**	**9678**	**16**	**54.8**	**9.2**

Data analysis and results

Accelerating and decelerating angular velocities were computed from video data by performing 2nd order polynomial curve fits on the frequency vs. time data and extracting the fitted curves' slopes at given frequencies (Figure 7). As the rotor is accelerating while suffering bearing loss, the sum of the angular acceleration and angular deceleration magnitudes is used in the calculation of unloaded torque and work done [3]:

$$\tau = J(\alpha_1 - \alpha_2) \qquad (2)$$

$$P_{out} = 2 \pi f \tau \qquad (3)$$

$$P_{in} = J_{flow} * \Delta P_{turbine} \qquad (4)$$

$$\text{efficiency} = P_{out} / P_{in} \qquad (5)$$

where τ is the torque (Nm), J is the moment of inertia of the rotor (kg m^2) which was derived from the geometry of the rotor components, α_1 and α_2 are the magnitude of acceleration and deceleration and f is the rotor rotational frequency (rev / s).

Figure 8 shows the frequency, acceleration, deceleration and unloaded torque curves for N3-R3 at 10 cc/s flow rate. Figure 9 shows the torque, power output and efficiency vs. rpm for the same system at different flow rates. Figure 10 compares the power output and efficiency vs. flow rate for four systems; N1-R1, N3-R3, N3-R2, N3-R1.

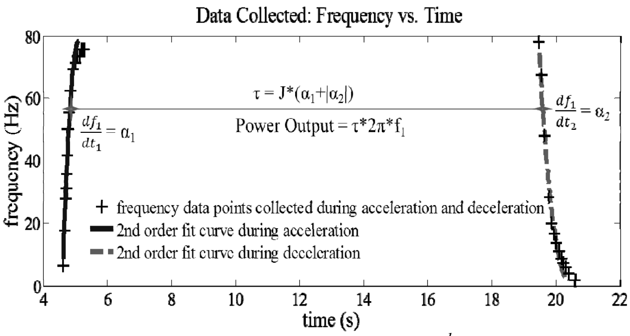

Figure 7: Sample raw video data (+), 2nd order polynomial curve fits for the acceleration (solid) and deceleration (dashed); slopes are α_1 and α_2. Torque (τ) and power output is calculated from α_1 and α_2.

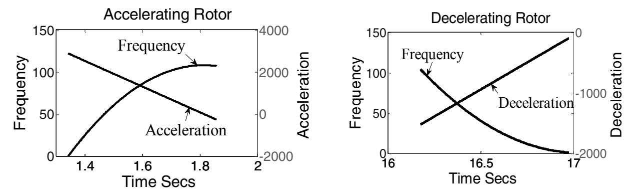

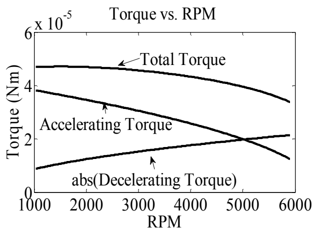

Figure 8: (top left) *rpm (solid) and angular acceleration (dash). (top right) rpm(solid) and angular deceleration (dash) (bottom left) acceleration , deceleration and unloaded torque vs. rpm for N3-R3 at 10 cc/s flow.*

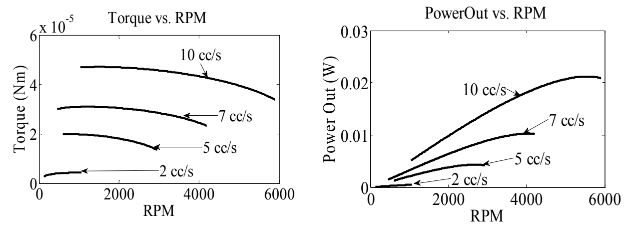

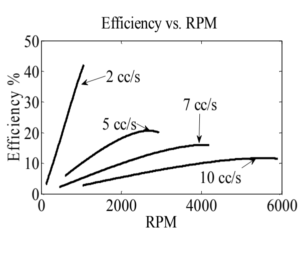

Figure 9: (top left) torque vs. rpm, (top right) power out vs. rpm, (bottom left) efficiency vs. rpm at different flow rates for N3-R3.

SUMMARY

Key findings and next steps

1. *Single nozzles* exhibited over 20% variation in efficiency within the tested range. In limited tests with 2 nozzles placed at 180 degrees from each other (using nozzles 4 and 8) we did not see a performance improvement. Further tests are needed at lower flow rates and with other nozzles.
2. Maximum efficiency was achieved at low flow rates. The 13 disk rotor stack (rotor3) realized 36% efficiency for 2 cc/sec flow rate at 0.4 mW power.
3. Higher gap "h" (rotor 3) and higher inner to outer radius ratio "r_i / r_o" (rotor 2) moved the efficiency peak to lower flow rates (with respect to rotor 1).
4. Nozzle 4, with the tangential entry angle to the rotor stack and an exit area 4% of the rotor inlet area (for rotor 1) achieved the highest power (45 mW) with 17% efficiency for 12 cc/sec flow rate.
5. High exit area (9% of rotor inlet area) and low exit area (0.8%) nozzles resulted in about 50% lower efficiency than the peak efficiency area (4%) nozzle.

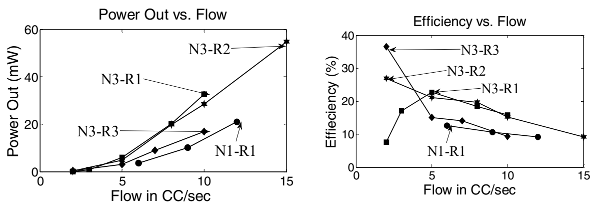

Figure 10 : (left) power out vs. flow; (right) efficiency vs. flow at maximum rpm for four systems.

Moving forward, we plan to model the loss mechanisms and perform parametric optimization of the design to enable 0.1 - 2 cm range Tesla turbine designs for given flow rate, head and power requirements.

REFERENCES:

[1] L. Taiz & E. Zeiger, *Plant Physiology*, Sinauer Associates, Inc., 4th edition, 2002.

[2] Ruba T. Borno, Joseph D. Steinmeyer, and Michel M. Maharbiz, "Charge-pumping in a synthetic leaf for harvesting energy from evaporation-driven flows" , *Applied Physics Letters*, 94,1 (2009)

[3] A Guha, B. Smiley, "Experiment and analysis for an improved design of the inlet and nozzle in Tesla disc turbines", *Proc. IMechE Vol. 224 Part A: J. Power and Energy, 261-277, Sept 2009*

[4] R.T.Deam et.al., "On Scaling Down Turbines to Millimeter Size", *Journal of Engineering for Gas Turbines and Power, v* 130 / 052301-9, September 2008.

[5] W Rice, "Tesla Turbomachinery," *Handbook of Turbomachinery*, CRC Press, 1994.

[6] Vince Romanin, Van P Carey, "Strategies for performance enhancement of Tesla turbines for combined heat and power applications", *Proceedings of the ASME 2010, 4th International conference on energy sustainability*, ES2010-19251, May 2010.

CONTACT

Vedavalli Krishnan, tel: 510-755-9640;
vedavalli@berkeley.edu